TECHNICAL ARTICLE

A Fractal Description of Finely Ground Particles of Natural Quartz Using Particle Size and Image Analyses

PEDRO L. GUZZO,[1] ŞTEFAN TĂLU [ID],[2,4] SLAWOMIR KULESZA,[3] and MIROSLAW BRAMOWICZ[3]

1.—Department of Mining Engineering, Federal University of Pernambuco, Recife, PE 50740-530, Brazil. 2.—The Directorate of Research, Development and Innovation Management (DMCDI), Technical University of Cluj-Napoca, 15 Constantin Daicoviciu St. Cluj County, 400020 Cluj-Napoca, Romania. 3.—Faculty of Technical Sciences, University of Warmia and Mazury in Olsztyn, Oczapowskiego 11, 10-719 Olsztyn, Poland. 4.—e-mail: stefan_ta@yahoo.com

The morphological characteristics of mineral particles in ultrafine range have a significant influence on engineering processes but have not been extensively explored until now. In this study, the morphology of fine quartz particles produced in a planetary ball mill is considered using fractal geometry and stereometric tools in connection with particle size analysis. Structure functions and bidimensional shape factors were derived from numerical analysis of scanning electron micrographs using surface height functions and watershed algorithms. Secondary electron images were obtained from aliquots of clear and milky quartz samples ground up to 32 h. The fragmentation fractal dimension derived from the uniformity index of particle size distributions showed a distinct non-monotonical increase with the elapsed grinding time for each sample. Overall variations in fractal parameters (fractal dimension and corner frequency) and Feret's diameter showed that the slowdown in particle size reduction and the onset of interparticle agglomeration occurred earlier for clear (monocrystalline) than for milky (polycrystalline) quartz. The onset of round-like agglomerates was also noticed with circular and round patterns. The loss of energy efficiency due to prolonged grinding processes was characterized by the decrease observed in the morphological fractal dimension.

INTRODUCTION

Particle size reduction is a key unit operation in numerous segments of chemical, ceramics, pharmaceutical and mineral processing systems responsible for significant energy consumption worldwide. During ultrafine grinding, i.e., the milling operation that grinds particles to $< 10~\mu$m, reliable particle separation is one of the biggest challenges due to the presence of surface forces.[1] This problem is critical in dry processes, in which the apparent grinding limit is achieved once agglomeration mechanisms exceed particle breakage via brittle microcracking.[2–4] Beyond that limit, a significant part of the mechanical energy delivered to the solid by means of grinding media is consumed for plastic deformation of crystalline grains.[5–7] Since the particulate system is continuously changing inside the mill compartment, the modeling of brittle-ductile mechanisms in large-scale industrial mills is technically impossible. The present study assumes that a detailed assessment of particle breakage and agglomeration resultant from comminution tests carried out in controlled laboratory conditions can be achieved if numerical approaches applied to digital images are adopted together with particle size analysis. As is known, intrinsic effects owing to particle size analysis such as dilution, stirring and ultrasound vibration are assumed to affect the particle size distribution (PSD) of dry ground powders. In this framework, image analysis can be an alternative method of

characterization of size, shape and surface roughness of particle systems independently from the above-mentioned effects related to particle size methods.[8–10]

After Turcotte[11] introduced the idea that breakage can be controlled by fractal geometry based on the notion of scale-invariant particle size ratios, the possibility to use fractal approaches to investigate the physical boundaries of particle systems has been currently considered in earth science and mineral engineering.[12–15] For instance, to clarify the fracture process responsible for the conversion of sedimentary quartz from sand to silt size range, Langroudi et al.[14] interpreted the propagation of latent microcracks and surface imperfections in quartz grains and consequent changes in PSD curves in terms of a fractal approach. Using experimental data obtained from particle impact breakage tests of marble in the 10–20 mm size range, Xu[15] showed that the fractal dimension of size distributions correlates positively with the applied stress and the specific fracture energy according to the Weibull statistics of particle failure. The fractal dimension of size distributions shows a ratio providing a statistical index of the fragmentation degree that varies with the intensity of particle size reduction.[13,16] In turn, the fractal dimension of surface shape (or surface roughness) represents the power-law shape-frequency distribution of progeny and accurately describes the surface topography of the ground product.[13,17] Compared to particle shape, the fractal analysis carried out in ground particles of sulfide ores showed that the surface roughness plays an important role in wettability and recovery of sulfide particles during the flotation process.[10] The importance of particle shape in mineral processing systems was highlighted by Little et al.[18] who investigated several aspects of quantitative analysis of digital images of finely ground multicomponent platinum ore such as the strengths and weaknesses of shape descriptors, the effects of image resolution and particle orientations and the sample statistics. To our best knowledge, similar studies using fractal analysis of ultrafine powders resultant from prolonged grinding tests of monomineralic particles such as quartz have not been carried out until now.

In addition to its technological importance in numerous segments,[19,20] crystalline quartz is often found in nature as large-size specimens free from accessory minerals, inclusions and porosities. The absence of cleavage planes can help the interpretation of general features governing size reduction and particle shape such as randomicity, stepwise and scale-length characteristics. Due to these attributes, quartz has always been considered a suitable material to assess fracture surface energy, specific energy consumption and PSD of daughter particles from comminution operations.[21–23] In the present study, fragmentation fractal approaches and stereometric methods are used to investigate morphological and size features of quartz fragments originated from prolonged dry grinding tests carried out in a planetary ball mill. Specifically, the evolution of fragmentation fractal dimensions and some shape descriptors were adopted to scrutinize the slowdown in grinding rate and the broadening in particle size distribution associated with the creation of strong agglomerates. These parameters were extracted from digital imaging processing of scanning electron micrographs (SEM) of powders resultant from dry grinding of clear (monocrystalline) and milky (polycrystalline) quartz fragments. The effect of quartz texture on size reduction and agglomeration is considered combining PSD and morphological fractal records.

MATERIALS AND METHODS

Samples

The samples investigated in this study were acquired from two distinct varieties of natural quartz from two provenances (Brazil): (1) clear (hyaline-like) euhedral specimens from a well-zoned pegmatite (Serra Branca, Cubati district; Paraiba); (2) massive blocks of milky quartz from a hydrothermal vein (Tanhaçu district, Bahia). SB and TA are the acronyms used throughout this study to label the ground aliquots for Serra Branca and Tanhaçu samples, respectively. The petrographic and mineralogical characterization of these samples can be summarized as follows: (1) the original fabric of SB is slightly twisted, fashioned with elongated bands without grain boundaries throughout the bulk volume; (2) TA has a polycrystalline texture fashioned with deformed primary grains (1800 μm $\pm$ 650 μm) surrounded by recrystallized grains (80 μm $\pm$ 45 μm); (3) the index of crystallinity estimated using the method proposed by Murata and Norman[24] is higher for SB (0.841 $\pm$ 0.010) compared to TA (0.752 $\pm$ 0.034), which can be easily explained by its monocrystalline texture; (4) the hyaline-like specimens show randomly vitreous fractures in the bottom of each crystal whereas the milky blocks show a preferential orientation of their macroscopic fracture pattern; (5) the Vickers hardness and fracture toughness of both samples assessed by the static indentation method are statistically the same.[25]

Griding Tests and Particle Size Analysis

The ground particles investigated in this study were produced by means of dry grinding carried out in a planetary ball mill (model Fritsch Pulverisette 5). The grinding medium was composed of 25 balls of zirconia (10 mm). Two bowls (250 ml) were used simultaneously, one for each sample. The charge volume and the revolution speed were fixed at 21 ml and 300 rpm, respectively. In total, 11 trials were completed with grinding time varying from 2 min to 1920 min (32 h).[25]
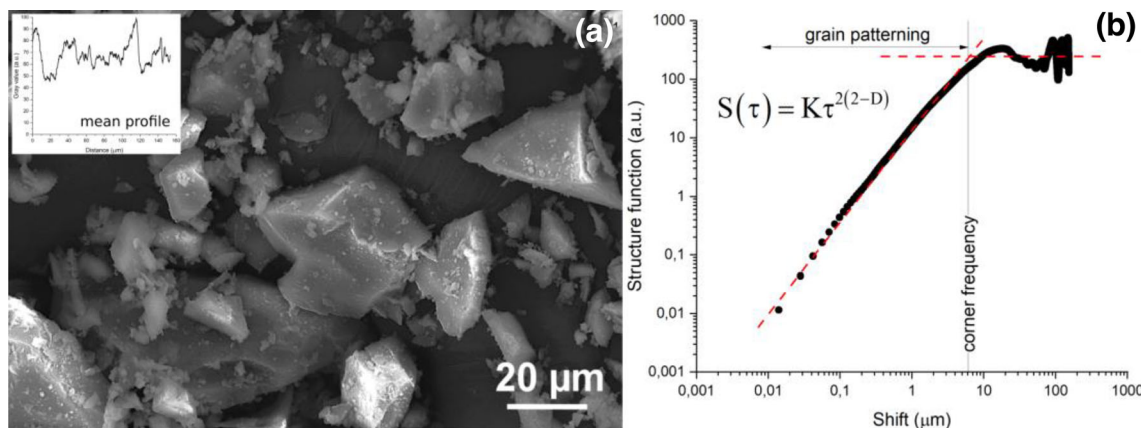
Fig. 1. (A) Typical SEM image of quartz ground particles (SB; 120 min) and the row-averaged mean profile (inset); (B) double log plot of the structure function vs. discrete shift obtained from the mean profile. The corner frequency delimits samples obeying allometric scaling behavior (grain patterning) within short-range surface bumps from the uncorrelated ones.

The particle size distributions employed for the present study were measured using laser light scattering (LLS) in Malvern Mastersizer 2000 equipment with the Hydro 2000 accessory using NaOH solution (pH 10) as a dispersant medium. The use of an alkaline solution helps to remove weakly bonded fines on the surface of partially broken quartz particles. Each ground sample was measured at least three times. Average diameters d_{50} were calculated that describe the apertures of the half of the passing particles. To evaluate the heterogeneity of the size distributions in the progeny of the fragments, the PSD curves were fitted with the empirical Rosin–Rammler (RR) function, which was found adequate in describing particle populations produced in ultrafine grinding processes.[26,27] This function takes the form:

$$R = 100 \cdot \exp[-(x/x_{63.2})^n] \quad (1)$$

where R is the cumulative percentage fraction of particles retained in each aperture x (in μm); $x_{63.2}$ is the reference size aperture associated with 63.2% of passing material and n is the uniformity index (n-index), which evaluates the heterogeneity of the size distribution. The reliability of the RR fitting was assessed by the coefficient of determination (R^2) that was always better than 0.99. In analogy with the power law exponent of Gaudin–Schuhmann distribution,[14] the fractal dimension for size distribution (D_S) of quartz powders was calculated in accordance with the relationship $D_S = 3 - n$, where the n-index corresponds to the slope of the PSD fitting line of RR function on a double logarithmic plot of accumulated fraction (R) versus the nominal aperture (x).

The morphology analyses of the particles ground for 2, 15, 120, 240, 480 and 1920 min were done using SEM images taken by JEOL-JSM-6460 microscope working with secondary electron beam (SE) excited with 30 kV voltage. The particles were coated with a thin gold layer to avoid charging. To track the progress of the morphological texture of the ground particles with the increase of the grinding time, each sample was carefully analyzed with the same sequence of magnifications, as follows: $100\times$, $400\times$, $800\times$, $1600\times$ and $3500\times$.

SEM Image Analysis

Secondary electrons appear because of inelastic scattering of the scanning beam in the sub-surface layers of the sample, and hence they provide useful information about topography of the sample's surface. During raster scan intensity of the secondary beam is converted to a grayscale number and written to a file. Hence, the pixels' values in SEM images can be thought of as pseudo-height entries from which one can obtain specific characteristics of the sample geometry. In this work SEM files were processed using two independent approaches that rely on: (1) scaling invariance behavior between samples of averaged surface profiles, the fractal approach, and (2) image segmentation into binarized selection areas, the statistical approach.

In the first method, row-averaged profiles along the fast-scanning axis were computed from the original SEM images (Fig. 1a and the inset therein). Obtained profile was then used to evaluate the structure function (shown in Fig. 1b) according to the formula:[28]

$$S(m) = \frac{1}{N-m} \sum_{n=1}^{N-m} (z_{n+m} - z_n)^2 \quad (2)$$

where m is the discrete shift between the mean profile and its copy, z_k is the k-th sample of the mean profile, and N is the number of scan steps along each profile. Thomas and Thomas[29] showed that one-dimensional structure function obeys allometric dependence upon the continuous independent variable, the scale length τ (Fig. 1b), as follows:

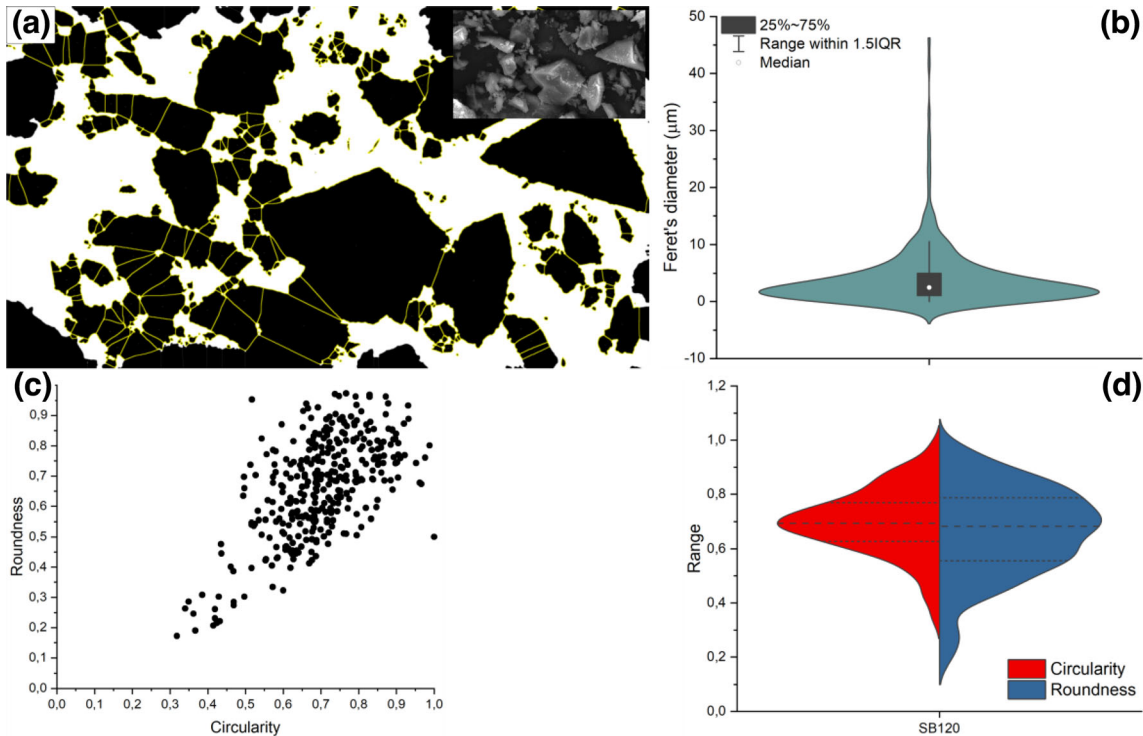$$S(\tau) = K\tau^{2(2-D)} \quad (3)$$

Fig. 2. Example results of stereometric characterization of the surface of quartz ground particles (SB; 120 min) using segmentation together with statistical analysis: (A) SEM image binarized using the watershed algorithm (original image shown in the inset); (B) violin plot showing the distribution of Feret's diameters determined in the binarized SEM image together with its statistical measures: median, interquartile range (IQR) and the lower/upper limits for the outliers; (C) scatter plot of the roundness vs. circularity data for the segments seen in the binarized SEM image; (D) split violin plot of the same circularity vs. roundness data exhibiting specific multimodal shapes of their distribution functions.

where D is the fractal dimension and K the pseudo-topothesy. Allometric dependence can be linearized in the double-log plot of the structure function against the scale length τ. Any sharp change in the slope of this plot is referred to as the corner frequency τ_c, which separates geometric objects of different scale-invariance characteristics.

In the second method, granular morphology of the surface was analyzed by means of stereometric analysis. To this end, SEM images were binarized using the watershed algorithm and obtained segments were then processed to determine specific shape descriptors: circularity, roundness and Feret's diameter. Circularity is a positive fractional number that exhibits the deviation from a perfect circle. It is calculated according to the formula:[28]

$$C = \frac{4\pi A}{P^2} \tag{4}$$

where A = is the segment area and P = its perimeter. When the circularity decays to zero, the segment becomes increasingly elongated; when it comes close to unity, the segment takes a perfect circular shape. Similar measure is roundness that equals the ratio of the lengths of the minor and the major axes of the best fit ellipse replacing given selection area expressed as follows:[28]

$$R = \frac{A}{\pi a^2} \tag{5}$$

where a is the semi-major axis of the equivalent ellipse. In turn, Feret's diameter determines the longest distance measured within the segment. Example results are shown in Fig. 2.

RESULTS AND DISCUSSION

Particle Size Distributions and SEM Images

Graphs of PSD functions of ground quartz particles measured from laser scattering are shown in Fig. 3. Dry grinding is found to give similar curves for both samples, clear/monocrystalline (SB) and milky/polycrystalline (TA), as it takes no longer than 120 min. In this time interval the peaks of both curves gradually shift to smaller particle size, whereas their width increases indicating enhanced size dispersion. With elapsed time, however, PSD becomes polydisperse: up to 480 min it is more evident for SB than for TA, whereas after 1920 min the opposite behavior can be seen. For the longest grinding, significant shift of the PSD to the right is clearly noticed for SB. Since particle size analysis was carried out in solution that enhances particle dispersion, the displacement of PSD towards the
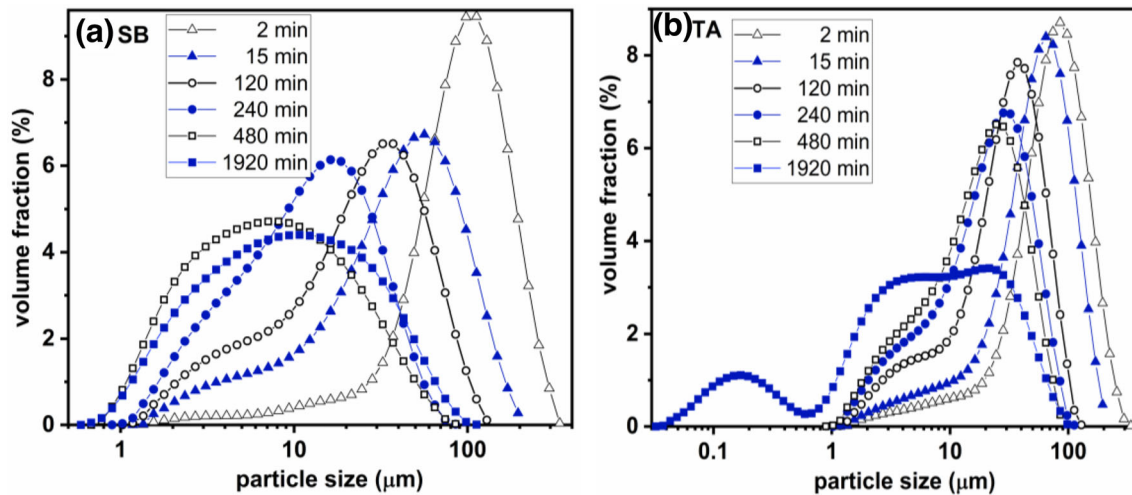
Fig. 3. Particle size distributions of quartz particles (a) SB: clear/monocrystalline; (b) TA: milky/polycrystalline - ground in a planetary ball mill at 300 rpm.

right indicates that the agglomerates formed with SB powders are more resistant against stirring and dilution steps than those formed with TA powders.

SEM images of quartz fragments subjected to fractal and statistical analyses are shown in Figs. 4 and 5. The values for the d_{50} diameter and the n exponent of the Rosin–Rammler equation determined from the PSD curves are also shown. The values for d_{50} and n calculated for the feed (the initial PSD before grinding) aliquots were, respectively, 108.4 μm $\pm$ 0.7 μm and 2.02 $\pm$ 0.03 for SB and 98.4 μm $\pm$ 1.3 μm and 1.92 $\pm$ 0.02 for TA. The size reduction factor (RF), defined as the ratio between d_{50} for feed and product, also shown in the images, is higher for SB mainly for the intermediate grinding times. The progress of the n-index confirms that the dispersion in PSD is increasing with the elapsed time of grinding. Since both samples show a slowdown in the n-index decreasing, the dispersion in size distribution does not growth monotonically with the increase of the grinding time. The plateau for the n-index close to 1.2–1.3 occurs much earlier for SB (15–240 min) compared to TA (240–480 min).

Analysis of SEM images shown in Figs. 4 and 5 helps to establish several observations on the morphology of the samples: (1) coarse feed particles are still observed in the SB aliquot ground for 15 min; (2) the edge-shaped pattern of fractured quartz is easily observed in SB sample, whereas cube-like morphology occurs in TB ground for 15 min and 120 min; (3) above 120 min, the pattern of sharp fragments is progressively substituted to a cloud of fine debris of undefined shape; (4) the change pointed out in (3) is evident for SB ground for 480 min; (5) the primary aggregation of fines on the surface of coarse fragments is helpful to explain the larger agglomerates observed in the SB aliquot ground for 1920 min; (6) the round agglomerates in Fig. 5f are likely responsible for the bimodal

distribution observed in Fig. 3b for TA ground for 1920 min.

As was previously observed for dolostone ground in similar conditions,[7] the adoption of prolonged periods in the dry grinding process was essential to produce large agglomerates with quartz powders. The experimental results shown here made clear that the kinetics of size reduction and agglomeration of quartz powders differ comparing the two types of samples upon investigation. The higher population of fine debris in the early stage of grinding and the higher concentration of surficial paramagnetic centers related to peroxy radicals were both proposed the as the main reasons for the occurrence of strong agglomerates in the ground product of clear (SB) quartz.[25] The lower grinding rates found for TA fragments were explained considering grain size and grain boundary barriers against propagation of microcracks that were observed in polycrystalline rocks.[30,31]

Fractal Dimension and Threshold Trends

Table I summarizes the fractal parameters derived from PSD and image analysis using surface height variations and allometric scaling invariance. Detailed results are also shown in the form of scatter plots in Fig. 6 as functions of the grinding time. In Fig. 6a, the fractal dimension of size distribution (D_S) is found to increase non-monotonically with the sharp upward steps observed in the following ranges: from min 2 to 15 min for SB and from 480 min to 1920 min for TA. The value of D_S varies from 1.19 to 2.30 in the entire range. Although the fractal dimension of the particle shape (D_R) approaches similar extreme values, the plots in Fig. 6b reveal their different trends upon grinding time. Within first 240 min the D_R value for SB decreases from 1.29 to 1.20 and then increases up to 1.31. For TA, a slight increase is observed from 1.25
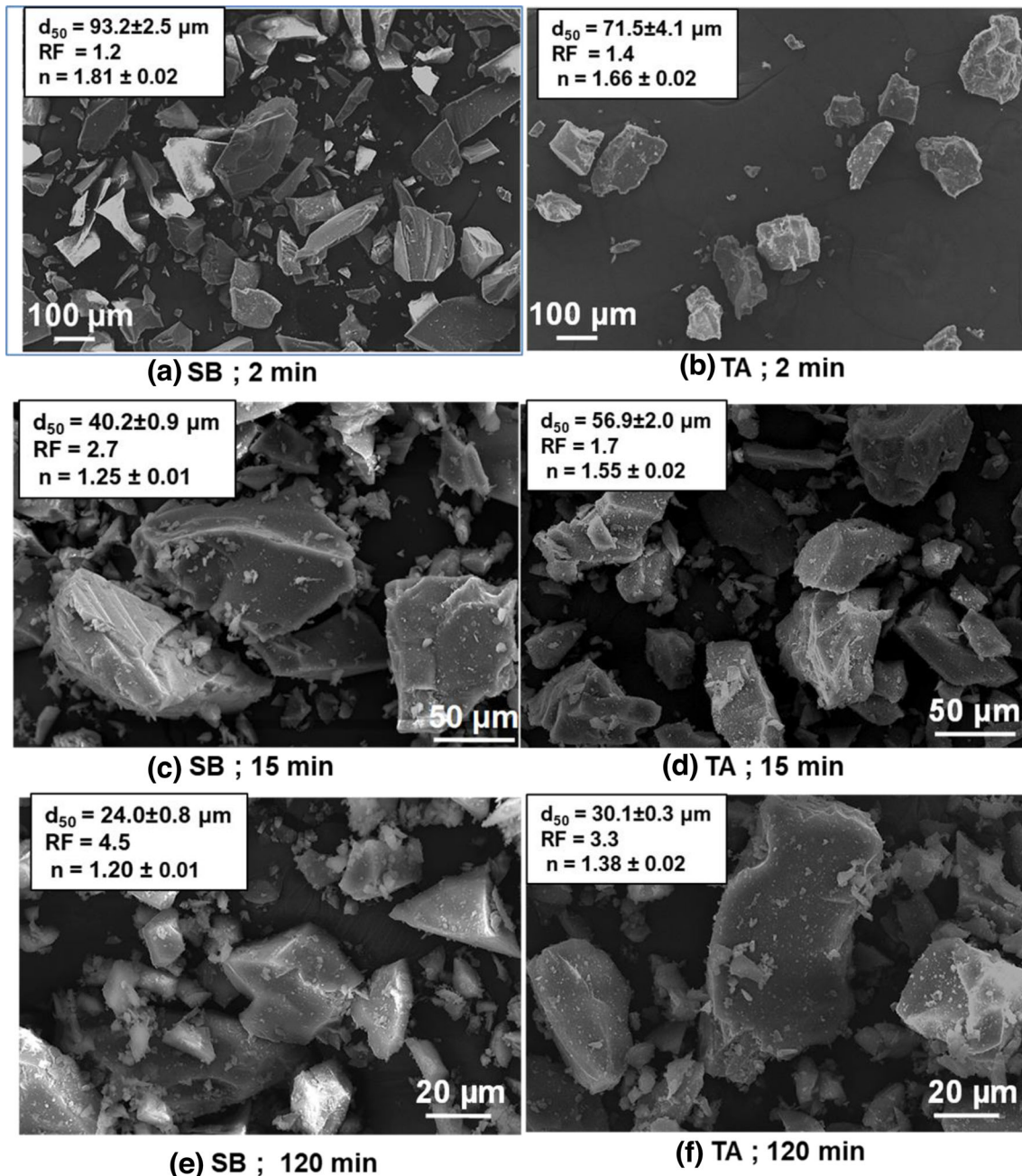
Fig. 4. SEM micrographs of SB (clear) quartz ground for: (a) 2, (c) 15 and (e) 120 min in a planetary ball mill at 300 rpm. SEM micrographs of TA (milky) quartz ground for: (b) 2, (d) 15 and (f) 120 min in a planetary ball mill at 300 rpm. The mean diameter (d_{50}) and the uniformity index (n) of the PSD are shown. The error corresponds to 1σ. RF: size reduction factor.

to 1.36, the highest value for this sample. For SB, the maximum in D_R (1.32) is attained in the 240–480 interval. As a result, two plateaus appear between 15 min and 480 min for SB: at 1.2 and 1.3. Above 480 min, the D_R value considerably decreases for both samples.

In semi-log plots, the fractal dimensions derived from PSD resultant from impact breakage tests follow linear trends with the specific energy and applied stress.[15–17,32] This trend occurs in low specific fracture energy comminution tests where

particle progeny results from few breakage events. Brown[33] observed that the interval of fractal dimension shift from [1.7–2.4] to [1.1–1.9] ranges when rock cores were fragmented using single and double impact test apparatus, respectively. This result was explained by an increase in the energy dissipation when particles were fragmented between two surfaces. Thus, the lower D_S and D_R values observed in our study can be explained because of multiple breakage mechanisms combining impact and friction forces inherent to planetary ball milling.[34]
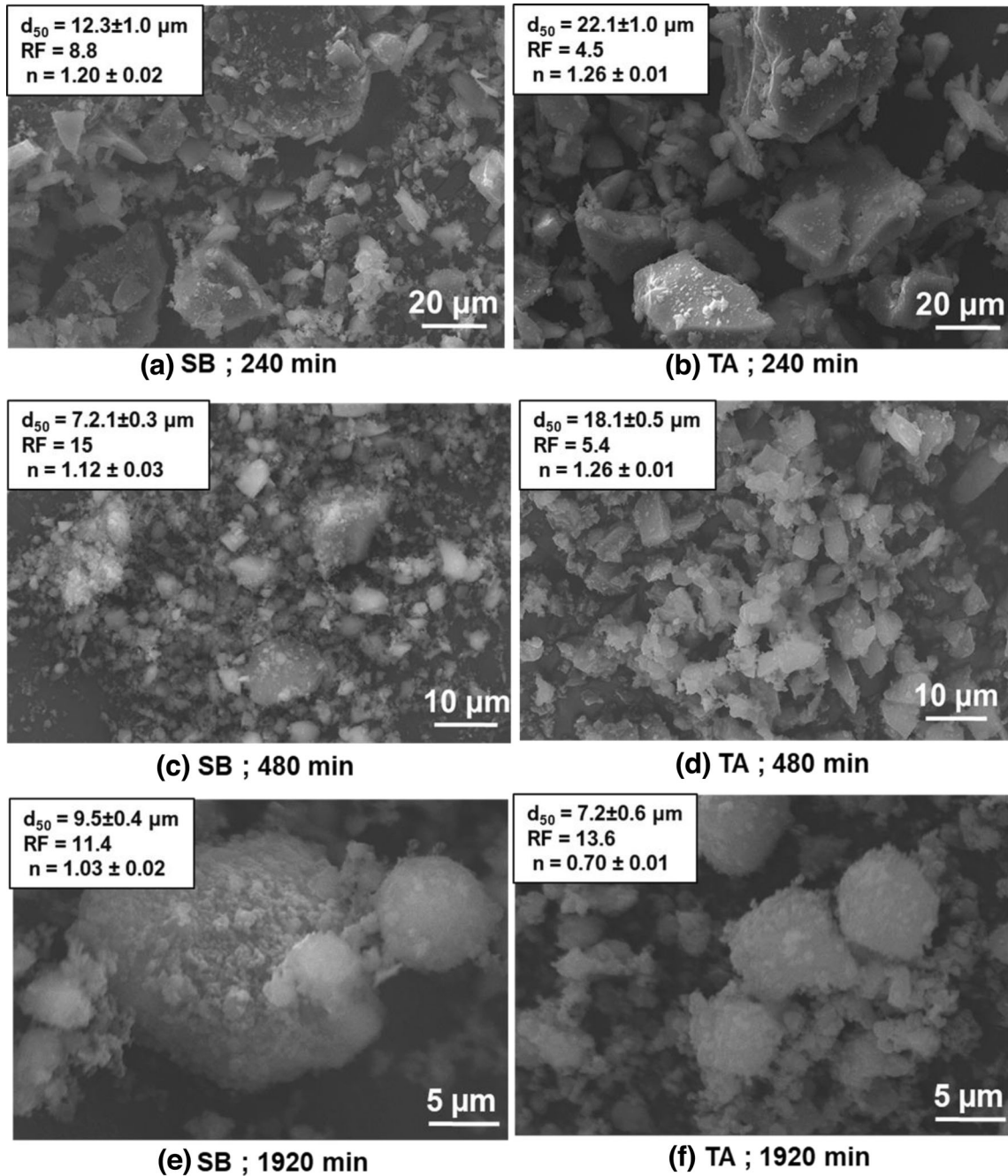
Fig. 5. SEM micrographs of SB (clear) quartz samples ground for: (a) 240, (c) 480 and (e) 1920 min in a planetary ball mill at 300 rpm. SEM micrographs of TA (milky) quartz samples ground for: (b) 240, (d) 480 and (f) 1920 min in a planetary ball mill at 300 rpm. The mean diameter (d_{50}) and the uniformity index (n) of the PSD are shown. The error corresponds to 1σ. RF: size reduction factor.

Previously, non-linear relationships between fragmentation fractal dimension and grinding time were observed for quartz sand ground in a vibrating mill[14] and soda-lime glass ground in a ball mill.[35] For quartz sand, it was observed that D_S quickly increases from 1.5 to 2.5 for the initial 3 min of the process. For longer times, slight variations around 2.5 were observed up to 12 min. In turn, for glass powder, D_S increases following three different slopes from 10 min to 120 min, similar to those in the SB plot in Fig. 6a. The slowdown in increasing

fractal dimension was explained by the loss of energy transfer with elapsed grinding time. In this framework, decrease in D_R observed in Fig. 6b for longer grinding times can be also explained in terms of energy dissipation related to competition between breakage and agglomeration events. The loss of energy efficiency is more evident for D_R vs. grinding time relationship probably because agglomeration registered with SEM analysis was not affected by dilution and stirring procedures.[36] Therefore, the lower dispersion resistance of agglomerates formed

Table I. Fractal dimensions related to PSD (D_S) and surface shape (D_R) and the corner frequency (τ_c) of particle patterns seen in SEM images of SB and TA samples at different grinding times

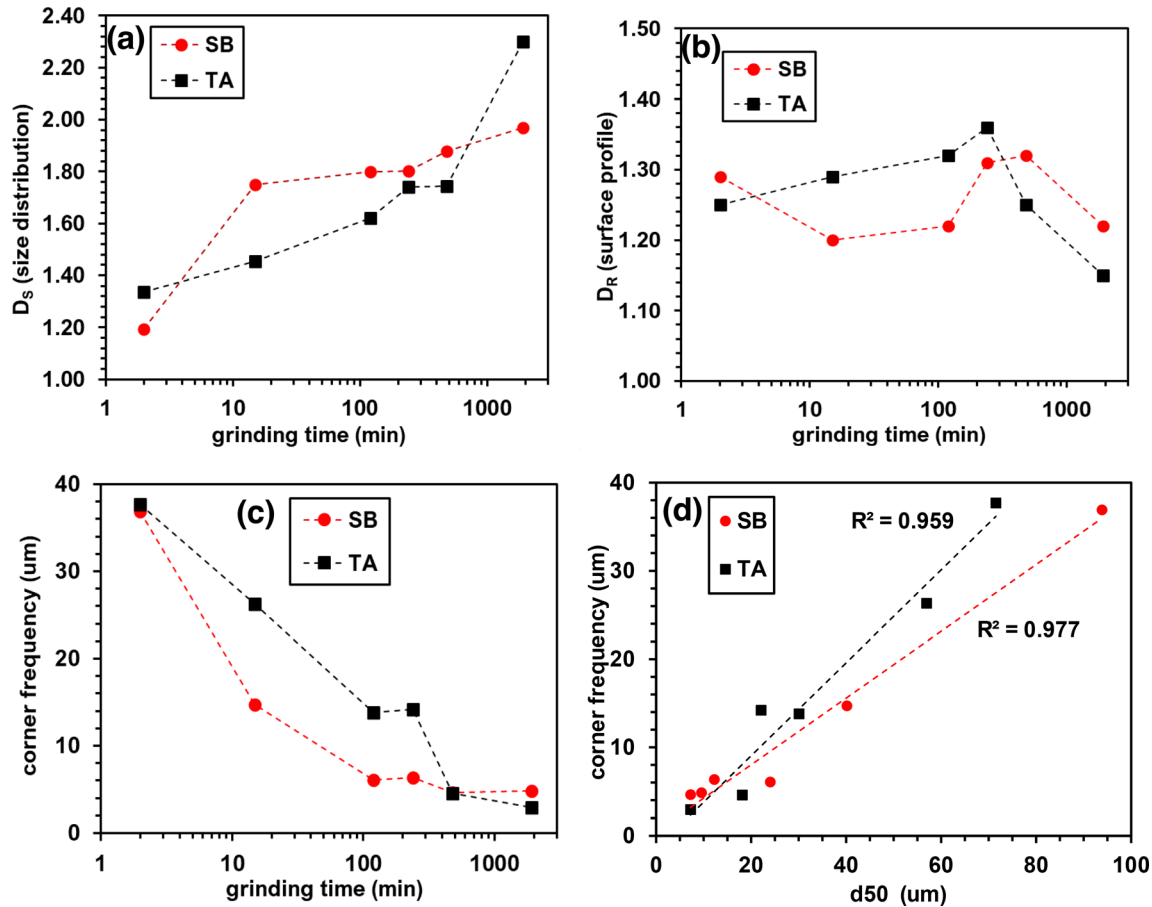| Grinding time (min)	SB			TA		
	D_S	D_R	τ_c (μm)	D_S	D_R	τ_c (μm)
2	1.19	1.29	36.9	1.34	1.25	37.7
15	1.75	1.20	14.7	1.46	1.29	26.3
120	1.80	1.22	6.07	1.62	1.32	13.8
240	1.80	1.31	6.34	1.74	1.36	14.2
480	1.88	1.32	4.63	1.74	1.25	4.59
1920	1.97	1.22	4.85	2.30	1.15	2.93

Fig. 6. Changes in fractal dimension (a, b) and corner frequency (c) of SB (clear) and TA (milky) quartz with elapsed time of the grinding process and the relationship between the corner frequency and the d_{50} diameter (d).

with TA powders generated after 1920 min is in accordance with abrupt D_S increasing shown in Fig. 6a. Since D_R was derived from SEM images, the loss of energy efficiency is mainly noticed in the last stage of grinding where agglomeration causes a net size increase in as-formed ground powders. The reliability of D_R to decode particle interaction and brittle-ductile transition in ultrafine grinding processes depends on further efforts to increase the statistical analysis of quartz SEM images and to

test the suggested methodology to other mineral-mill systems.

The graph shown in Fig. 6c exhibits a non-monotonical decrease in the corner frequency (τ_c) as a function of the grinding time. According to previous study of Tălu et al.,[37] corner frequency in monofractal structures roughly equals the diameter of dominant particles on the surface, and hence it can be a measure of the particle size. To verify this statement for the materials under study, the

relationships between τ_c and d_{50} are shown in Fig. 6d. Although τ_c and d_{50} do not vary in the same range of values, linear relationships with satisfactory R^2 fitting factors were found for both samples. In fact, τ_c is numerically similar to d_{10}, the characteristic diameter related to the aperture of 10% of passing material, which decreases from 33.7 μm to 2.1 μm for SB and from 22.6 μm to 0.3 μm for TA. Hence, the gradually decreasing τ_c observed in Fig. 6c confirms the slowdown of the particle size with the elapsed time of grinding. A similar relationship was also observed for τ_c versus d_{10}, which confirms the monofractal trend of finely ground quartz.

The slope in the τ_c plot up to 120 min is higher for SB compared to TA. This result agrees well with the higher grinding rates calculated for SB using an empirical energetic model based on particle size and grinding time.[25,34] Comparison of d_{50}, d_{10} and τ_c values leads to the conclusion that the decay in the particle size with elapsed grinding time is different for each sample. Looking at the data in Fig. 6c, the threshold can be seen at around 240 min, where both graphs sharply change their slope. Note that this threshold corresponds to the onset of plateau in Fig. 6b, which suggests qualitative change in the evolution of the particle morphology at this stage of the grinding process.

Shape Factor and Morphological Trends

Table II summarizes averaged shape descriptors of surface height variations (circularity, roundness and Feret's diameter) that were derived by means of image segmentation algorithm followed by statistical analysis carried in SEM images. The variation of these parameters as a function of the grinding time and the size reduction factor are shown in Fig. 7.

As seen in Fig. 7a, mean circularity in SB sample varies between 0.67 and 0.75 during the grinding process similar to TA sample, except for the large gap seen at 240 min. Even closer trends are seen in Fig. 7b, where the roundness graphs are presented. In this case, both scatter plots follow almost flat lines at the value 0.67 with the values for TA systematically lower than the respective SB values below 480 min. On the other hand, changes in mean

Feret's diameter with elapsed grinding time shown in Fig. 7c reveals asymptotic decay from ca. 40/70 μm down to 0.6/0.7 μm for SB/TA samples, respectively. Obtained results are akin to those presented in Fig. 6c for the corner frequency. On average, the decrease in Feret's diameter can be approximated by exponential decay function similar to that in the energetic empirical model used to estimate grinding rate and grinding limit for these samples.[25,34]

The decay of Feret's diameter with size reduction factor estimated from PSD shown in Fig. 7d is significantly different for each sample. As observed in Fig. 7c, the decay of Feret's diameter observed for TA quartz confirms a three-step breakage with negligible variations for grinding between 15 min and 240 min. In turn, a two-step breakage including higher reduction factors is noticed for SB quartz up to 480 min. Above this stage, the change in the trend of the size reduction factor and slowdown in Feret's diameter are further evidence of the significance of agglomeration of small fragments of SB quartz.

Aside from mean stereometric characteristics of the segments in binarized SEM images, it is also interesting to have insight into the evolution of their distribution functions. To this end, Fig. 8 shows split violin plots of circularity/roundness vs. grinding time that demonstrate geometric homogeneity of the detected segments in terms of their shape rather than size. Circularity and roundness data of the SB sample in the upper row in Fig. 8 show predominant unimodality within 120 min of the grinding process. With elapsed time, however, a morphological change occurred reflected by the unimodal distribution associated with the appearance of almost round particles (circularity and roundness close to the unity) together with larger content of distorted particles (circularity and roundness close to 0.7). The onset of round particles noticed in this analysis confirms the onset of the agglomeration process revealed for PSD and fractal analysis. In case of the TA sample (lower row in Fig. 8) similar transition occurred later, between 480 min and 1920 min, but the final picture is similar: a powder composed of a mixture of almost

Table II. Mean shape characteristics (circularity, roundness and Feret's diameter) of particles detected in SEM images of quartz samples (SB and TA) at different grinding stages

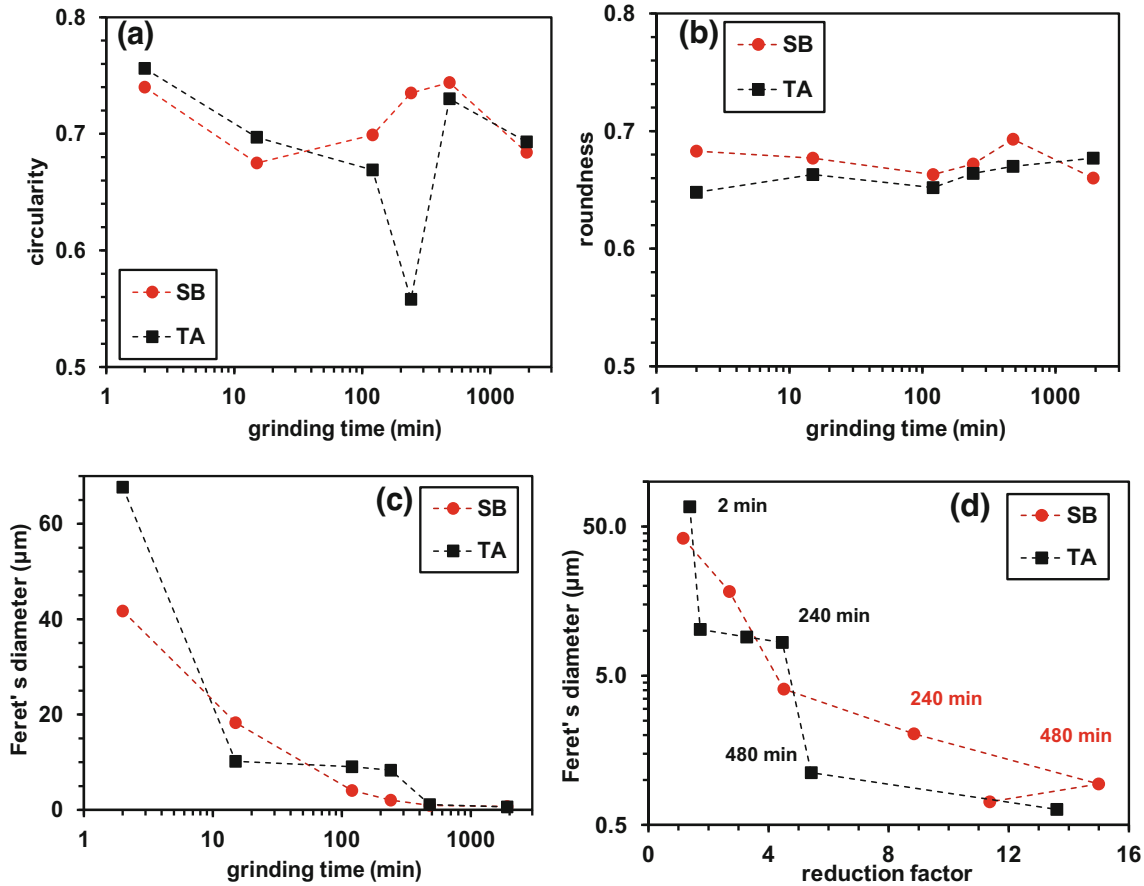| Grinding time (min)	SB			TA		
	Circularity	Roundness	Feret's diameter (μm)	Circularity	Roundness	Feret's diameter (μm)
2	0.740	0.683	41.7	0.756	0.648	67.7
15	0.675	0.677	18.3	0.697	0.663	10.2
120	0.699	0.663	4.06	0.669	0.652	9.07
240	0.735	0.672	2.04	0.588	0.664	8.34
480	0.744	0.693	0.940	0.730	0.670	1.12
1920	0.684	0.660	0.715	0.693	0.677	0.636

Fig. 7. Changes in: (a) circularity, (b) roundness and (c) Feret's diameter (shape descriptors of binarized segments) of SB (clear) and TA (milky) quartz samples with the elapsed grinding time. (d) The relationship between the Feret's diameter and size reduction factor of SB (clear) and TA (milky) quartz samples.
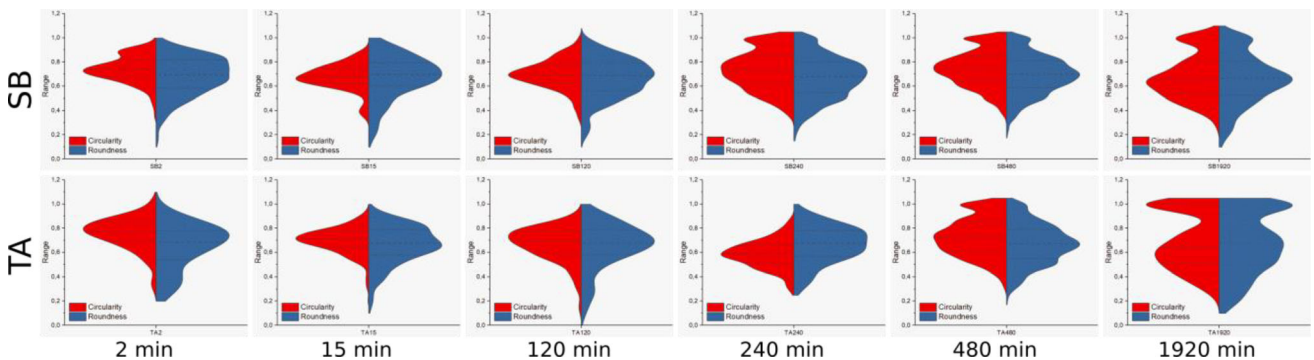

Fig. 8. Changes in distribution functions of the circularity (are shown in red color in the left side of the vertical axis) and roundness (are shown in blue color in the right side of the vertical axis) of area segments detected in binarized SEM images of SB and TA samples (upper and bottom rows, respectively) during the grinding process (from left to right) shown in the form of split violin plots (Color figure online).

circular and distorted particles (circularity and roundness close to 0.6). Previously, Little et al.[18] observed that the capability of circularity for categorizing the shape of particles with different sizes in finely ground platinum ore was worse than that of roundness. This divergence was explained in terms of a higher sensitivity of the perimeter measurement in relation to image resolution compared to the area measurement that is used for roundness calculation. Since similar particle shape distributions were found for circularity and roundness, the number of pixels per particle image used to decode quartz particles with the elapsed time of grinding was satisfactory.
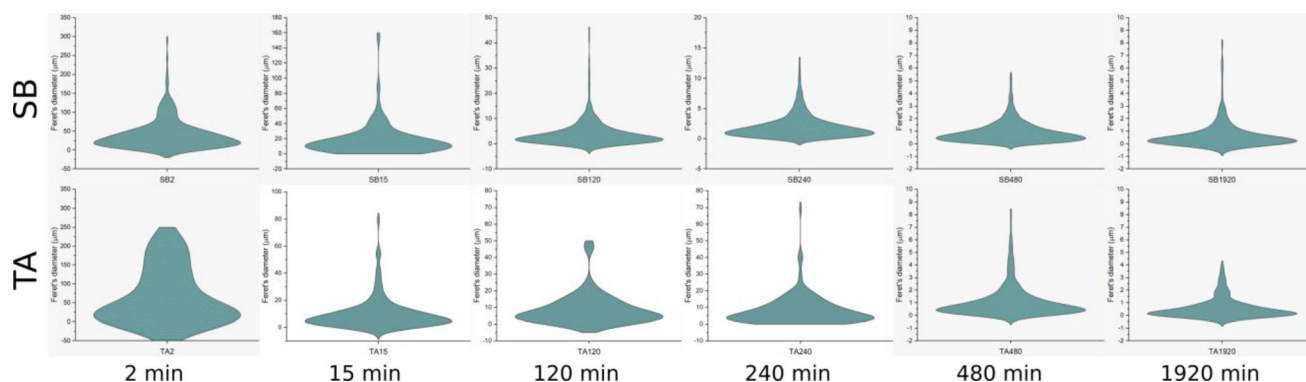
Fig. 9. Changes in distribution density data of Feret's diameter of segments detected in binarized SEM images of SB and TA samples (upper and bottom rows, respectively) during the steps of the grinding process (from left to right) shown in the form of violin plots.

For the complete picture, Fig. 9 shows violin plots of the distribution functions of Feret's diameter data determined from binarized SEM images of the samples at different steps of the grinding process. In the beginning the distributions appear wide (up to 250 μm), even though they peaked at very low values (around 20 μm). With elapsed time, however, the distribution functions became thinner and more symmetric and end up with peak Feret's diameter at a few hundred nanometers. Note that at this stage the powder is a mixture of round/distorted particles (Fig. 8), so it can be concluded that all the above-mentioned particles are of similar size. Above 480 min, obtained powders are therefore homogeneous in terms of their particles' size but not the shape. This clearly disagrees with the broadening of the PSD (Fig. 4) and the decrease in the uniformity index (n-index) obtained from the Rosin–Rammler function. Observed discrepancy can be explained by partial dispersion of the as-produced agglomerates during sample preparation for analysis with laser scattering. The fact that laser scattering methods assume spherical particles might be included as well.[36] Although numerically smaller than d_{50}, Feret's diameter seems more appropriate to decode the actual size of as-produced agglomerates.

CONCLUSION

The evolution of fragmentation fractal dimensions and shape descriptors probed in intensely ground quartz fragments with mono- and polycrystalline textures and linked to particle size analysis can be concluded as follows:

(1) The monofractal structure of quartz powder samples varied in different ways with elapsed grinding time. Sharp increase in fractal dimension of size distributions occurred at short grinding time for monocrystalline fragments (15 min) and at much longer periods (> 480 min) for polycrystalline fragments. Changes in fractal dimension and corner frequency values confirmed that the polycrys-

talline texture of milky quartz offered a higher fracture resistance during the planetary milling process.

(2) The higher grinding rates found for monocrystalline fragments of clear quartz and the earlier formation of strong agglomerates seen from particle size analysis were both confirmed observing the corner frequency evolution and the distribution functions of circularity and roundness data. Thus, the use of fractal parameter and shape descriptors in conjunction can be useful to characterize the progress of finely ground monomineralic particles in dry milling processes where agglomeration mechanisms play an important role in particle size and distributions.

(3) After long grinding periods (> 240 min), the loss of the energy transfer due to the competition between breakage and agglomeration mechanisms at the micro-scale was recognized observing the decrescent behavior in the fractal dimension. Assuming suitability of the sampling procedure, this method appears to be more accurate for quantitative sizing of as-ground agglomerates because of dilution and stirring effects inherent to laser scattering methods.

AUTHOR CONTRIBUTIONS

PLG: Conceived the experimental work, methodology, SEM imaging, drafted the manuscript. ŞT:

Conceived the study, revised the manuscript. SK: Fractal analysis, investigation, supervision. MB: Draft preparation, data analyses, investigation, validation. All authors have read and agreed to the published version of the manuscript.

DATA AVAILABILITY

The data that support the findings of this study are available from the corresponding author upon reasonable request.

CONFLICT OF INTEREST

On behalf of all authors, the corresponding author states that there is no conflict of interest. The funders had no role in the design of the study; in the collection, analyses, or interpretation of data; in the writing of the manuscript, or in the decision to publish the results. No author has a financial or proprietary interest in any material or method mentioned.

REFERENCES

1. W. Peukert, H.C. Schwarzer, and F. Stenger, *Chem. Eng. Process.* 44, 245 (2005).
2. L. Opoczky, *Powder Technol.* 17, 1 (1977).
3. C. Knieke, M. Sommer, and W. Peukert, *Powder Technol.* 195, 25 (2009).
4. P. Przibara, S. Breitung-Faes, and A. Kwade, *Adv. Powder Technol.* 29, 416 (2018).
5. V.V. Boldyrev, S.Y. Pavlov, and E.L. Goldberg, *Int. J. Miner. Process.* 44–45, 181 (1996).
6. Q. Zhang, J. Kano, and F. Saito, in *Handbook of Powder Technology*, vol 12. ed. by A.D. Salman, M. Ghadini, and M.J. Hounslow (Elsevier, Amsterdam, 2007), pp. 509–528.
7. P.L. Guzzo, F.B.M. de Barros, and A.A.A. Tino, *Powder Technol.* 342, 141 (2019).
8. T.P. Meloy, and M.C. Williams, *Challenges in Mineral Processing* (SMI, New York, 1994), pp. 207–221.
9. F. Podczeck, *Powder Technol.* 93, 47 (1997).
10. M.M. Ahmed, *Int. J. Miner. Process.* 94, 180 (2010).
11. D.L. Turcotte, *J. Geophys. Res.* 91, 1921 (1986).
12. B.H. Kaye, G.G. Clark, and Y. Liu, *Part. Part. Syst. Charact.* 9, 1 (1992).
13. A. Thomas, and L.O. Filippov, *Int. J. Miner. Process.* 57, 285 (1999).
14. A.A. Langroudi, I. Jefferson, K. O'hara-Dhand, and I. Smalley, *Geomorphology* 211, 1 (2014).
15. Y. Xu, *Powder Technol.* 323, 337 (2018).
16. G.J. Brown, N.J. Miles, and T.F. Jones, *Miner. Eng.* 9, 715 (1996).
17. H. Nagahama, *Int. J. Rock Mech.* 30, 469 (1993).
18. L. Little, M. Becker, J. Wiese, and A.N. Mainza, *Miner. Eng.* 82, 92 (2015).
19. P.L. Guzzo, in *Rochas & Minerais Industriais: Usos e Aplicações*, 2nd edn. ed. by A.B. Luz, and F.F. Lins (CETEM, Rio de Janeiro, 2008), pp. 681–721. (**in Portuguese**).
20. J. Götze, in *Quartz: Deposits, Mineralogy and Analytics*. ed. by J. Götze, and R. Möckel (Springer, Berlin Heidelberg, 2012), pp. 1–28.
21. K. Yildirim, H. Cho, and L.G. Austin, *Powder Technol.* 105, 210 (1999).
22. D.W. Fuerstenau, and A.-Z.M. Abouzeid, *Int. J. Miner. Process.* 67, 161 (2002).
23. L.M. Tavares, in *Handbook of Powder Technology*. ed. by A.D. Salman, M. Ghadini, and M.J. Hounslow (Elsevier, Amsterdam, 2007), pp. 3–68.
24. K.J. Murata, and M.B. Normann II., *Am. J. Sci.* 276, 1120 (1976).
25. P.L. Guzzo, F.B. Marinho de Barros, B.R. Soares, and J.B. Santos, *Powder Technol.* 368, 149 (2020).
26. J. Yue, and B. Klein, *Miner. Eng.* 18, 325 (2005).
27. A. Shrivastava, S. Sakthivel, B. Pitchumani, and A.S. Rathore, *Powder Technol.* 211, 46 (2011).
28. Ş Tălu, *Micro and Nanoscale Characterization of Three Dimensional Surfaces. Basics and Applications* (Napoca Star Publishing House, Cluj-Napoca, 2015).
29. A. Thomas, and T.R. Thomas, *J. Wave Mater. Interact.* 3, 341 (1988).
30. E. Eberhardt, B. Stimpson, and D. Stead, *Rock Mech. Rock Eng.* 32, 81 (1999).
31. N.G. Yilmaz, Z. Karaca, R.M. Goktan, and C. Akal, *Constr. Build. Mater.* 23, 370 (2009).
32. S. Sadrai, J.A. Meech, D. Tromans, and F. Sassani, *Miner. Eng.* 24, 1053 (2011).
33. G.J. Brown, *Miner. Eng.* 10, 229 (1997).
34. H. Mio, J. Kano, and F. Saito, *Chem. Eng. Sci.* 59, 5909 (2004).
35. S. Liu, Q. Li, G. Xie, L. Li, and H. Xiao, *Powder Technol.* 295, 133 (2016).
36. C.O.R. Abbireddy, and C.R.I. Clayton, *Proc. Inst. Civil Eng. Geotech. Eng.* 162, 193 (2009).
37. Ş Tălu, M. Bramowicz, S. Kulesza, A. Shafiekhani, A. Ghaderi, F. Mashayekhi, and S. Solaymani, *Ind. Eng. Chem. Res.* 54, 8212 (2015).